

Force-free current-induced reentrant melting of the vortex lattice in superconductors

Sergey Savel'ev,¹ Ciro Cattuto,¹ and Franco Nori^{1,2,*}

¹Frontier Research System, The Institute of Physical and Chemical Research (RIKEN), Wako-shi, Saitama 351-0198, Japan

²Center for Theoretical Physics, Department of Physics, CSCS, University of Michigan, Ann Arbor, Michigan 48109-1120

(Received 4 March 2003; published 30 May 2003; publisher error corrected 14 August 2003)

When increasing a current j flowing along the vortex lines, we obtain both a gradual shift of the vortex-lattice melting transition (VLMT) to a lower magnetic field and also a rising reentrant melting line, both separating the vortex solid from the vortex-liquid phase. The upper branch of the VLMT merges with the predicted reentrant lower branch at a certain value j_{merge} of the force-free current. We also derive the entire VLMT diagram in (B, T, j) three-dimensional phase space, and propose possible applications of it—including a magnetic-sensitive current-controlled switch using $\text{Bi}_2\text{Sr}_2\text{CaCu}_2\text{O}_{8+\delta}$ tapes.

DOI: 10.1103/PhysRevB.67.180509

PACS number(s): 74.25.Dw

Thermal vortex fluctuations in high-temperature superconductors are responsible for the “vortex-lattice melting transition” (VLMT). A vortex liquid can exist at both relatively high and low magnetic fields, resulting in a reentrant VLMT (Refs. 1,2) for decreasing magnetic field B [see, e.g., Fig. 1(a)]. Such a reentrant VLMT is very difficult to observe experimentally because it occurs at very low fields and even very weak pinning freezes the dilute vortex-liquid phase.¹

Similarly, a force-free current j (i.e., applied along the vortices) tends to destabilize the vortex lattice. In an infinite superconductor with no pinning, helical vortex spirals are unstable for any value of the force-free current and the vortex lattice cannot exist. However, boundary effects and/or vortex pinning stabilize^{3–7} the vortex-solid for low j .

In general, the elasticity of the vortex lattice, softened by a small applied force-free current, can resist thermal fluctuations, so that the vortex lattice survives in a region of the B - T - j phase diagram. Note that both a force-free current and thermal noise often coexist in experiments, and indeed it was observed that the VLMT field decreases with increasing force-free current.^{8,9} This result is consistent with our calculations and with Ref. 7.

Here, we find that the competition among the Lorentz force induced by the force-free current, thermal noise, and elasticity can result in a *reentrant vortex-lattice melting* with *decreasing* magnetic field [Figs. 1(b) and 2(a–c)]. This occurs for much stronger vortex pinning and much higher magnetic fields as compared to the usual reentrant VLMT^{1,2} [Fig. 1(a)]. The reentrant transition found here provides a remarkable case of field-induced superconductivity (FIS) in samples loaded by a force-free current. Indeed, there is a low- B region in (j, B) phase space, where, on increasing B , the vortex lattice melts and resistivity sharply drops.

To date, the important phenomenon of FIS has only been observed in a few exotic superconductors^{10,11} and was associated with the “cancellation” of the applied external magnetic field H by an effective field produced by ion spins. A somewhat similar idea, of compensation of the external magnetic field by an internal field, has been realized using a nanoengineered lattice of magnetic dots on top of a superconducting film.^{12,13} In this interesting system,¹² the interplay of the external magnetic field and the field generated by the nanomagnets with magnetization $m||H$ shifts the super-

conducting region on the H - T phase diagram to higher positive (if $m > 0$) or negative (if $m < 0$) magnetic fields. Changing the magnetization m of the dots, the field interval $H_{\text{crit}}^{\text{low}}(m, T) < H < H_{\text{crit}}^{\text{high}}(m, T)$ where superconductivity exists can be controlled. Note that this superconducting state is strongly nonuniform (“Swiss-cheese” structure), since the normal state sets in directly under the nanomagnets, where the local magnetic field is high. Here we predict that, in contrast to Ref. 12, a macroscopically *uniform* superconducting state (vortex-solid phase) occurs within the interval $H_{\text{melt}}^{\text{low}}(j, T) < H < H_{\text{melt}}^{\text{high}}(j, T)$ for a sample loaded by a force-free current j . The predicted temperatures *and* melting fields for $\text{Bi}_2\text{Sr}_2\text{CaCu}_2\text{O}_{8+\delta}$ are much *higher* than the measured values for the nanomagnet-superconductor structures in Refs. 12 and 13: the FIS presented in Ref. 12 is observed at $T = 5\text{--}7$ K and $H \leq 30$ Oe. Moreover, here the range $(H_{\text{melt}}^{\text{low}}, H_{\text{melt}}^{\text{high}})$ can be easily tuned by varying j and T , while $(H_{\text{crit}}^{\text{low}}, H_{\text{crit}}^{\text{high}})$ in Ref. 12 can only be changed by resetting the magnetization. More importantly, our proposal does *not* require complex nanoengineering capabilities, which are not easily accessible to most experimental groups.

In order to construct the (B, T, j) VLMT phase diagram for a superconductor loaded by a force-free current, we first obtain the elastic free energy of the vortex-solid array. Straight vortices (the z axis is chosen to be parallel both to the vortex lines and the applied current) do not feel the current flowing along them. However, as soon as a vortex line is curved, say due to thermal noise, the current component perpendicular to the local vortex orientation generates the Lorentz force $\mathbf{f}_l = (\Phi_0 j / c) [\mathbf{e}_z \times \partial \mathbf{u} / \partial z]$. Here, Φ_0 is the flux quantum, c the speed of light, \mathbf{e}_z the unit vector along the z axis, and \mathbf{u} the local displacement of the vortex segment from its equilibrium position on a triangular lattice of straight vortex lines. The Lorentz force provides a quadratic contribution,^{4,7} with respect to the displacements \mathbf{u} , to the free energy $\mathcal{F}_{el} = \int \Phi_{\alpha\beta}(\mathbf{k}) u_\alpha(\mathbf{k}) u_\beta(-\mathbf{k}) d^3\mathbf{k} / (16\pi^3) - B j \int i k_z [u_x(\mathbf{k}) u_y(-\mathbf{k}) - u_x(-\mathbf{k}) u_y(\mathbf{k})] d^3\mathbf{k} / (8c\pi^3)$, where $\Phi_{\alpha\beta}(\mathbf{k})$ is the elastic matrix (see, e.g., Ref. 5). The vector $\mathbf{k}_\perp = (k_x, k_y)$, perpendicular to the z axis, runs over the first Brillouin zone of the vortex lattice, which is usually approximated by the circle: $k_x^2 + k_y^2 = k_\perp^2 < K_0^2 = 4\pi B / \Phi_0$. The wavelength of the \mathbf{u} -displacement waves propagating along vorti-

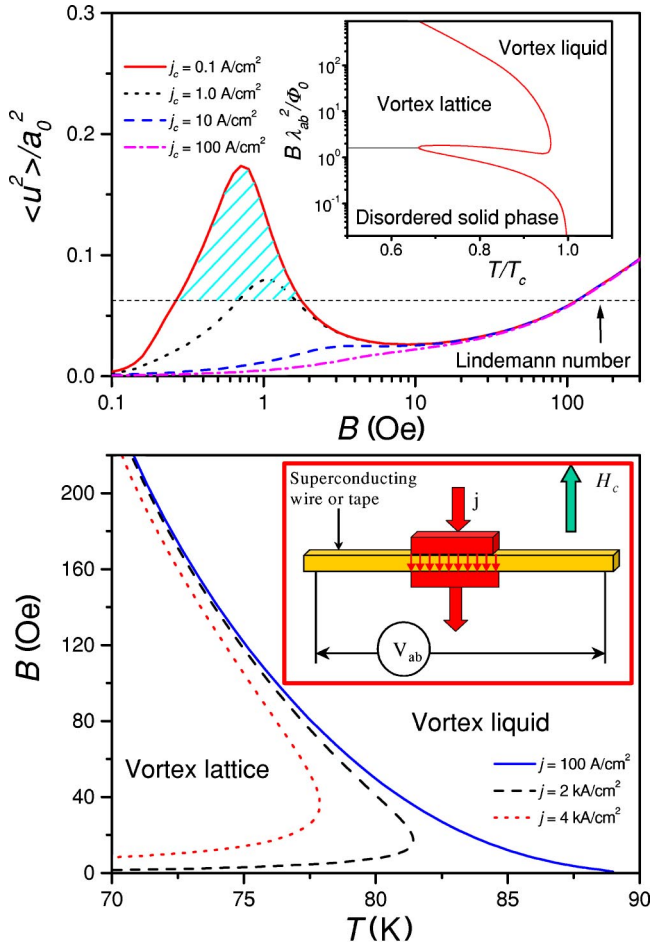


FIG. 1. (Color online) (a) The ratio $\langle u^2 \rangle / a_0^2$ versus B for $j=0$ and different values of j_c . Inset in (a): the known “noselike” (B, T) phase diagram of the vortex-lattice melting transition for $j_c = 0.1$ A/cm 2 . (b) (B, T) phase diagrams for different force-free currents and $j_c = 100$ A/cm 2 . There is no reentrant VLMT at low j , but the reentrant branch of the VLMT appears for $j=4$ and 2 kA/cm 2 . The parameters in (a) and (b) are representatives of Bi $_2$ Sr $_2$ CaCu $_2$ O $_{8+\delta}$ ($\gamma=200, \lambda_{ab}=2000/\sqrt{1-T^2/T_c^2}$ Å, $T_c=90$ K). Inset in (b): a sketch of a current-controlled field-sensitive switch.

ces cannot be smaller than the out-of-plane coherence length ξ_c for continuous anisotropic superconductors or the distance s between CuO $_2$ planes for layered superconductors. Thus, $|k_z| \leq k_z^{\max} \leq \min(\pi/s, 1/\xi_c)$. The above equation for \mathcal{F}_{el} can be interpreted as a softening of the rigidity of the vortex-lattice caused by the force-free current.

The homogeneous force-free current configuration (for the nonhomogeneous case, see Ref. 14) does not involve interactions between vortex phonons \mathbf{u} having different wave vectors, i.e., the free energy \mathcal{F}_{el} is diagonal in the \mathbf{k} representation. This allows us to calculate exactly different thermodynamic quantities, including the mean-square displacement of vortices from their equilibrium positions. The latter is determined by the path integral $\langle (u(\mathbf{r}_0))^2 \rangle = (1/Z) \int \mathcal{D}u(\mathbf{r}) (u(\mathbf{r}_0))^2 \exp(-\mathcal{F}_{el}/T)$, where $Z = \int \mathcal{D}u(\mathbf{r}) \exp(-\mathcal{F}_{el}/T)$ is the partition function. Calculating the Gaussian integral, the mean-square displacement $\langle u^2 \rangle$ can be expressed as an ordinary integral over \mathbf{k} space:

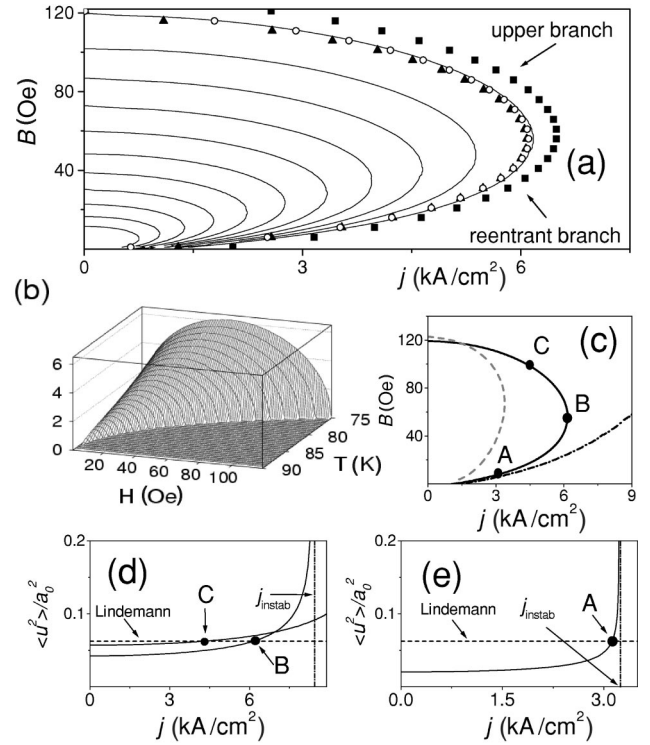


FIG. 2. (a) (B, j) phase diagrams at different temperatures from $T=75$ to 85 K in steps of 1 K. The parameters are the same as in Fig. 1, with $j_c=100$ A/cm 2 . Two branches can be seen: an upper branch $B_{\text{melt}}^{\text{high}}(j)$ and a lower reentrant branch $B_{\text{melt}}^{\text{low}}(j)$. The solid squares and triangles represent the (B, j) phase diagram for different pinning strength $j_c=500$ and 20 A/cm 2 . The large difference in critical currents results in a minor difference in (B, j) phase diagram. Moreover, if we neglect pinning ($j_c=0$) and take into account the finite thickness $l_c \approx 1.5$ μm of the sample along the c axis (by restricting the integration region to $k_z > k_z^{\min} \approx 1/l_c$), a (B, j) phase diagram was obtained (open circles) which basically coincides with the one for $j=100$ A/cm 2 . (b) The three-dimensional (B, T, j) VLMT phase diagram. (c) The (B, j) VLMT phase diagram at $T=75$ K: as computed numerically (solid line), and as estimated via the transcendental equation (dashed line, $\beta=3$). The integral (1) diverges along the dash-dotted line. Parts (d) and (e) show j scans of $\langle u^2 \rangle / a_0^2$ for $B=8$ Oe (A), 55 Oe (B), and 100 Oe (C), also marked in part (c).

$$\langle u^2 \rangle = T \int \frac{d^3 \mathbf{k}}{(2\pi)^3} \frac{\Phi_{xx} + \Phi_{yy}}{\Phi_{xx} \Phi_{yy} - \Phi_{xy}^2 - B^2 j^2 k_z^2 / c^2}. \quad (1)$$

In order to obtain a concrete VLMT phase diagram, we now restrict ourselves to the case of an anisotropic layered superconductor, with the external field \mathbf{B} along the c axis. In this case, the elastic matrix can be expressed via the \mathbf{k} -dependent elastic moduli and the Labusch parameter α_L describing vortex pinning: $\Phi_{xx} = c_{11}k_x^2 + c_{66}k_y^2 + c_{44}k_z^2 + \alpha_L(\mathbf{k})$, $\Phi_{yy} = c_{66}k_x^2 + c_{11}k_y^2 + c_{44}k_z^2 + \alpha_L(\mathbf{k})$, $\Phi_{xy} = \Phi_{yx} = (c_{11} - c_{66})k_x k_y$. The compression $c_{11}(\mathbf{k})$, shear c_{66} , and tilt $c_{44}(\mathbf{k})$ elastic moduli are listed in Ref. 15 and have standard forms (see Ref. 5). The Labusch parameter α_L can be approximated¹⁶ by $\alpha(\mathbf{k}) \approx B j_c / (2c r_p)$, where j_c is the critical current density for

$B \perp j_c$ and r_p the radius of the pinning potential. The weak-pinning contribution to the elastic response is essential to suppress the unbounded growth of long-pitch spirals that would otherwise occur in an infinite pin-free sample. Note that for a vanishing force-free current the integrand appearing in Eq. (1) can be written as the sum of two terms, namely, $1/(C_{66}k_{\perp}^2 + C_{44}k_z^2 + \alpha)$ and $1/(C_{11}k_{\perp}^2 + C_{44}k_z^2 + \alpha)$, for compression-free and rotation-free waves, respectively. However, a force-free current couples these waves.

The Lindemann criterion and its modifications have been commonly used to study the melting of several vortex-solid phases (see, e.g., Ref. 17). Moreover, the applicability of this criterion was validated in the frame of more fundamental theoretical approaches (e.g., Ref. 18), as well as—more importantly—via good agreement with a variety of experimental data on VLMT (see, e.g., Ref. 19). Therefore, we can use the Lindemann criterion $c_L^2 a_0^2 = \langle u^2 \rangle$ with intervortex distance $a_0 \approx \sqrt{\Phi_0/B}$ to study how the applied current affects the VLMT, with the Lindemann number c_L , usually chosen in the interval 0.1–0.3. First, we present a rough analytical estimate of $\langle u^2 \rangle$ to clarify the physical picture. Afterwards, we present numerical calculations of the integral (1), taking into account *all* contributions to the elastic matrix in Ref. 15.

After several calculations, outlined in Ref. 21, we obtain the transcendental equation for the VLMT magnetic field: $c_L^2 = \langle u^2 \rangle / a_0^2 = cTB(\bar{U}_{11} + 2\bar{U}_{44}) \ln[(\bar{U} + Bjk_z^*/c)/(\bar{U} - Bjk_z^*/c)] / (2\pi\Phi_0^2 j \bar{U})$. Here, we use the compression $\bar{U}_{11} = B^2/(4\pi\lambda_{ab}^2)$ and the electromagnetic tilt stiffness \bar{U}_{44} , $\bar{U} \approx B(\bar{U}_{44})^{1/2}/(2\sqrt{\pi}\lambda_{ab}) \approx (\Phi_0)^{1/2} B^{3/2} [\ln(1 + 4\lambda_{ab}^2/c_L^2 a_0^2)]^{1/2} (8\pi\sqrt{2}\pi\lambda_{ab}^3)^{-1}$, and renormalize the maximum k_z as $k_z^* \sim \gamma/\lambda_{ab}$, γ being the anisotropy. At high B , so that $jk_z^*/c \ll \bar{U}/B \propto \sqrt{B}$, the influence of the current j on $\langle u^2 \rangle$ is negligible and the ratio $\langle u^2 \rangle / a_0^2$ decreases with decreasing B as $32\pi\lambda_{ab}^4 B T k_z^* / \Phi_0^3 \ln(1 + 4\lambda_{ab}^2/c_L^2 a_0^2)$. Thus, it satisfies the Lindemann condition at a certain melting field if the force-free current is not too strong. However, on further decreasing B , the current j becomes relevant as soon as \bar{U}/B approaches jk_z^*/c . This results in a strongly increased mean-square displacement $\langle u^2 \rangle$, which, in this approximation, diverges logarithmically at $\bar{U}/B = jk_z^*/c$. Therefore, the value of $\langle u^2 \rangle$ exceeds $c_L^2 a_0^2$ also in this case, and we can expect a “reentrant melting transition” with decreasing magnetic field. The physical reason of this reentrant VLMT branch is the suppression of the stability of the vortex-lattice phase by means of force-free currents favoring short-pitch ($1/k_z^*$) spirals.

In the zero-current limit ($j \rightarrow 0$), we are able to reproduce the upper branch of the VLMT, $B_{\text{melt}}^{\text{high}} = c_L^2 \Phi_0^3 [\ln(1 + 4\lambda_{ab}^2/c_L^2 a_0^2)]^{1/2} / (32\pi\gamma T \lambda_{ab}^3)$ if we take (consistent with Ref. 2) $\bar{U}_{11} \gg \bar{U}_{44}$ and choose the maximum k_z exactly as in Ref. 2: $|k_z^*| = \gamma [\ln(1 + 4\lambda_{ab}^2/c_L^2 a_0^2)]^{1/2} / \lambda_{ab}$. However, we cannot obtain the usual very low- B reentrant branch in the (B, T) VLMT phase diagram at $j=0$ because now we only keep the short-range contribution \bar{U}_{44} to the tilt energy $C_{44}k_z^2$ (which should be replaced by $\Phi_0^2 k_z^2 / 70\pi^4 \lambda_{ab}^4$ for small k_z) and neglect the shear elasticity. Therefore, it is clearly seen that the usual reentrant melting is completely different from the pro-

posed one, and our obtained behavior is robust with respect to the strength of the pinning. Thus, in order to get more accurate results, we perform numerical calculations of the integral (1) using all of the elastic moduli listed in Ref. 15. For zero force-free current, both the upper and the usual reentrant (B, T) branches of the VLMT are recovered. Namely, the ratio $\langle u^2 \rangle / a_0^2$ decreases with decreasing B and becomes equal to the Lindemann number (hereafter, $c_L = 0.25$) at a certain VLMT field. Then the value of $\langle u^2 \rangle / a_0^2$ reaches a minimum and starts to increase again, attaining a maximum at low field [Fig. 1(a)]. If the height of this maximum is over the Lindemann number [see shaded area in Fig. 1(a)], the vortex-lattice melts again. Because of pinning, on further decreasing B this vortex liquid freezes into a disordered solid phase with small thermal fluctuations, $\langle u^2 \rangle / a_0^2 < c_L^2$. The maximum of $\langle u^2 \rangle / a_0^2$ is strongly suppressed with increasing pinning, as shown in Fig. 1(a). Thus, the low-density vortex liquid becomes completely frozen even at very weak pinning. The (B, T) VLMT phase diagram for very weak pinning is shown in the inset of Fig. 1(a).

Beyond being consistent with known results [Fig. 1(a)], we present the complete B - T phase diagram [Fig. 1(b)] for different values of the force-free current j , using a reasonable value of the critical current density $j_c = 100$ A/cm². We choose these large j_c 's in order to suppress the usual reentrant melting and to consider only the behavior associated with the force-free current. For the chosen value of j_c , no VLMT reentrant transition is observed at the lowest considered value of the force-free current j . However, the reentrant transition appears if a high-enough current is applied along B , as expected from our analytical consideration. Next, the (B, j) phase diagram is constructed at different temperatures [Fig. 2(a)]. For all temperatures, this phase diagram also exhibits a reentrant behavior with decreasing B : the liquid phase is found at both low $B < B_{\text{melt}}^{\text{low}}(j)$ and high $B > B_{\text{melt}}^{\text{high}}(j)$, while the ordered vortex-lattice phase exists for intermediate fields $B_{\text{melt}}^{\text{low}}(j) < B < B_{\text{melt}}^{\text{high}}(j)$. At a certain value j_{merge} of the force-free current, these two branches merge. Thus, the vortex-lattice phase cannot set in at $j > j_{\text{merge}}$. Computing (B, j) phase diagrams at different temperatures T , the three-dimensional (B, T, j) phase diagram is built [Fig. 2(b)].²²

The role of thermal fluctuations and spiral instabilities can be recognized in j scans of $\langle u^2 \rangle / a_0^2$ [Figs. 2(d) and 2(e)]. Along the upper branch $B_{\text{melt}}^{\text{high}}(j)$, and close to the merging current $j_{\text{merge}}(B)$, the value $\langle u^2 \rangle / a_0^2$ exceeds the Lindemann number far from the current $j_{\text{instab}}(B)$ [dash-dotted curve in Fig. 2(c)], where the “helical” instability occurs. This can be clearly seen in the j scans shown in Fig. 2(d), corresponding to points C and B on Fig. 2(c). For low magnetic fields [point A in Fig. 2(c)], the helical instability becomes more relevant, causing melting near the instability threshold $j = j_{\text{instab}}(B)$ [see also j scan in Fig. 2(e)].

The obtained reentrant behavior of the VLMT with decreasing B , in the presence of a force-free current, can be easily verified experimentally, for instance, investigating the behavior of the magnetization jump associated with the VLMT. Also, in-plane or out-of-plane transport measure-

ments may show a reviving resistance on lowering the applied magnetic field. This work could also apply to the vortex state of He^4 under the action of a superfluid flow along vortices.²³ It is important to stress that the “usual” reentrant behavior² has not been observed in $\text{Bi}_2\text{Sr}_2\text{CaCu}_2\text{O}_{8+\delta}$, despite intensive experimental studies of the VLMT up to very weak magnetic fields (see, e.g., Ref. 24). This is because the shear elasticity becomes weak enough for the reentrant melting to occur only at very low fields: $B \approx 10^{-3} \Phi_0 / \lambda_{ab} (T=0) \approx 0.5$ Oe. We predict a reentrant melting, in the presence of a force-free current, for magnetic fields that are two orders of magnitude higher. This occurs because of the competition of the spiral instability with the tilt vortex rigidity. More importantly, this melting is tunable and can be effectively controlled by the intensity of the force-free current.

Regarding applications, the FIS effect predicted here can be utilized for *magnetic-sensitive current-controlled switches*, for devices that need to operate within a certain interval of magnetic fields, as well as for logical devices. For

instance, a switch [inset in Fig. 1(b)] could be made from a $\text{Bi}_2\text{Sr}_2\text{CaCu}_2\text{O}_{8+\delta}$ film or wire placed in a magnetic field parallel to the c axis and locally loaded by a c -axis current. Such a switch has very low in-plane resistivity R_{ab} in the superconducting (vortex-solid) phase, while R_{ab} sharply increases in the vortex-liquid phase. Thus, this switch is “on” in-between the magnetic fields $H_{\text{melt}}^{\text{low}}$ and $H_{\text{melt}}^{\text{high}}$ (continuously tuned by j and T), and it is “off” otherwise. In conclusion, the VLMT in a sample loaded by a force-free current was studied analytically and numerically in the (B, T, j) parameter space. It was found that the VLMT shifts to a lower magnetic induction with increasing current and, remarkably, that a reentrant melting transition also occurs when further decreasing the applied magnetic field. Our proposal might have potential applications for magnetic-sensitive current-controlled electrical switches.

We gratefully acknowledge support from the US National Science Foundation under Grant No. EIA-0130383.

*Email address: nori@umich.edu

¹G. Blatter *et al.*, Rev. Mod. Phys. **66**, 1125 (1994).

²G. Blatter *et al.*, Phys. Rev. B **54**, 72 (1996).

³J.R. Clem, Phys. Rev. Lett. **38**, 1425 (1977).

⁴E.H. Brandt, J. Low Temp. Phys. **44**, 33 (1981).

⁵E.H. Brandt, Rep. Prog. Phys. **58**, 1465 (1995).

⁶Y.A. Genenko, Phys. Rev. B **53**, 11 757 (1995).

⁷M. Kohandel and M. Kardar, Phys. Rev. B **61**, 11 729 (2000).

⁸C.D. Keener *et al.*, Phys. Rev. Lett. **78**, 1118 (1997).

⁹S. Ooi, T. Mochiku, and K. Hirata, Physica C **362**, 269 (2001); **378-381**, 523 (2002); J. Mirković, *et al.*, *ibid.* **378-381**, 428 (2002); M. Charalambous *et al.*, Phys. Rev. B **45**, 5091 (1992).

¹⁰H.W. Meul *et al.*, Phys. Rev. Lett. **53**, 497 (1984).

¹¹S. Uji *et al.*, Nature (London) **410**, 908 (2001); L. Balicas *et al.*, Phys. Rev. Lett. **87**, 067002 (2001).

¹²M. Lange *et al.*, cond-mat/0209101 (unpublished).

¹³Y. Otani *et al.*, J. Magn. Magn. Mater. **126**, 622 (1993).

¹⁴S. Savel'ev *et al.*, Physica C **378-381**, 495 (2002).

¹⁵For $H \parallel c$ axis, the elastic moduli are $C_{11} = (1 + \lambda_c^2 k^2) \Gamma(\mathbf{k}) / (1 + \lambda_{ab}^2 \mathbf{k}^2)$; $C_{44} = \Gamma(\mathbf{k}) + U_{44}/k_z^2$, $U_{44} = 2 \epsilon_0 [\ln[(1 + \lambda_{ab}^2 (\tilde{k}_z^2 + K_0^2)) / (1 + \lambda_{ab}^2 K_0^2)] + k_z^2 \lambda_{ab}^2 \gamma^{-2} \ln[\xi_{ab}^{-2} \lambda_c^2 / (1 + \lambda_c^2 K_0^2 + \lambda_{ab}^2 k_z^2)]]$; $C_{66} \approx \epsilon_0 \lambda_{ab}^2$ for $a_0 < \lambda_{ab}$, and $C_{66} \approx \epsilon_0 \lambda_{ab}^2 (a_0 / \lambda_{ab})^{3/2} \times \exp[-a_0 / \lambda_{ab}]$ for $a_0 > \lambda_{ab}$. Here, $\epsilon_0 = B \Phi_0 / (64 \pi^2 \lambda_{ab}^4)$, $\Gamma(\mathbf{k}) = B^2 / [4 \pi (1 + \lambda_c^2 k_{\perp}^2 + \lambda_{ab}^2 k_z^2)]$, λ_{ab} and λ_c are the in-plane and out-of-plane penetration depths, ξ_{ab} is the coherence length, $\gamma > 1$ the anisotropy parameter, and $a_0 \approx \sqrt{\Phi_0 / B}$. According to Refs. 2 and 25 the logarithm in the first term of U_{44} should be cut at $\tilde{k}_z \approx \min(k_z, 2/\sqrt{\langle u^2 \rangle})$ instead of k_z ; this is important in the vicinity of the VLMT, where displacements can be quite large.

¹⁶L. Glazman and A. Koshelev, Phys. Rev. B **43**, 2835 (1991).

¹⁷G. Mikitik and E.H. Brandt, Phys. Rev. B **64**, 184514 (2001); D. Ertas and D.R. Nelson, Physica C **272**, 79 (1996).

¹⁸C. Dasgupta and O.T. Valls, Phys. Rev. Lett. **87**, 257002 (2001); H. Nordborg and G. Blatter, Phys. Rev. B **58**, 14 556 (1998).

¹⁹C.M. Aegerter *et al.*, Phys. Rev. B **57**, 14 511 (1998).

²⁰S.L. Lee *et al.*, Phys. Rev. B **55**, 5666 (1997).

²¹In the case of extremely anisotropic ($\gamma \gg 1$) layered superconductors, the compression elastic response can be approximated as $C_{11} \mathbf{k}_{\perp}^2 \approx \bar{U}_{11} = B^2 / (4 \pi \lambda_{ab}^2)$ for $\mathbf{k}_{\perp}^2 \geq 1 / \lambda_{ab}^2$. In this case, the main contribution to the elastic tilt energy $C_{44} k_z^2$ is related to the electromagnetic interaction of pancake vortices forming pancake stacks. Thus, we can assume $C_{44} k_z^2 \approx \bar{U}_{44}$, with the \mathbf{k} -independent electromagnetic tilt stiffness $\bar{U}_{44} = \Phi_0 B / (32 \pi^2 \lambda_{ab}^4) \ln(1 + 4 \lambda_{ab}^2 / c_L^2 a_0^2)$. This approximation of the tilt elastic energy remains valid as long as the second term of U_{44} ,¹⁵ associated with the Josephson coupling between PV's, does not exceed the first electromagnetic term. In analogy to Ref. 2, we can roughly take this into account by renormalizing the maximum value of the z component as $|k_z| < k_z^* = \min(k_z^{\text{max}}, \tilde{k}_z)$, where $\tilde{k}_z = (\gamma / \lambda_{ab}) \{ \beta \ln(1 + 4 \lambda_{ab}^2 / c_L^2 a_0^2) / \ln[1 / (4 \pi \xi_{ab}^2 / a_0^2 + 2 \xi_{ab}^2 / \lambda_c^2)] \}^{1/2} \sim \gamma / \lambda_{ab}$, with $\beta \geq 1$. In addition, recognizing that the VLMT occurs in strongly anisotropic materials such as $\text{Bi}_2\text{Sr}_2\text{CaCu}_2\text{O}_{8+\delta}$ at low magnetic fields, $B_{\text{melt}} \lesssim \Phi_0 / \lambda_{ab}^2$ (see, e.g., Ref. 20), we can neglect the shear contribution to the elastic matrix. Hence, in this approximation, the mean-square displacement is determined by the expression: $\langle u^2 \rangle \approx T f(d^3 \mathbf{k} / 8 \pi^3) (\bar{U}_{11} + 2 \bar{U}_{44}) / (\bar{U}^2 - B^2 j^2 k_z^2 / c^2)$, where $\bar{U} \equiv \{ \bar{U}_{44} (\bar{U}_{11} + \bar{U}_{44}) \}^{1/2}$ and here we neglect pinning. The last integral is easily calculated, yielding the transcendental equation for the VLMT magnetic field presented in the text.

²²Comparing the analytical and numerical results [Fig. 2(c), dashed and solid curves], the vortex-lattice phase persists at higher currents than it is expected from the transcendental equation for the melting field. This nonessential discrepancy between our numerical and analytical results is due to having dropped the tilt elasticity associated with the Josephson coupling (second term of U_{44}) in our analytical approach. It is important to stress that the present results are robust with respect to the detailed way of introducing pinning and/or surface effects [see Fig. 2(a)].

²³T. Araki, M. Tsubota, and C. F. Barenghi, Physica B **329-333**, 226 (2003).

²⁴A. Oral *et al.*, Phys. Rev. Lett. **80**, 3610 (1998).

²⁵J. Clem, Phys. Rev. B **43**, 7837 (1991).